Hydrology and Earth System Sciences

Open Access

Discussions

Modeling the effect of glacier recession on streamflow response using a coupled glacio-hydrological model

B. S. Naz[1,*], C. D. Frans[1], G. K. C. Clarke[2], P. Burns[3,], and D. P. Lettenmaier[1]**

[1]Civil and Environmental Engineering, University of Washington, Seattle, WA, USA
[2]Earth, Ocean and Atmospheric Sciences, University of British Columbia, Vancouver, BC, Canada
[3]Department of Geosciences, Oregon State University, Corvallis, OR, USA
[*]now at: Oak Ridge National Lab, Oak Ridge, TN, USA
[**]now at: Watershed Sciences Inc., Portland, OR, USA

Correspondence to: D. P. Lettenmaier (dennisl@uw.edu)

HESSD

10, 5013–5056, 2013

Modeling the effect of glacier recession on streamflow response

B. S. Naz et al.

Title Page

Abstract	Introduction
Conclusions	References
Tables	Figures

|◄ | ►|
◄ | ►

Back | Close

Full Screen / Esc

Printer-friendly Version

Interactive Discussion

Abstract

We describe an integrated spatially distributed hydrologic and glacier dynamic model, and use it to investigate the effect of glacier recession on streamflow variations for the Upper Bow River basin, a tributary of the South Saskatchewan River. Several re-
5   cent studies have suggested that observed decreases in summer flows in the South Saskatchewan River are partly due to the retreat of glaciers in the river's headwaters. Modeling the effect of glacier changes on streamflow response in river basins such as the South Saskatchewan is complicated due to the inability of most existing physically-based distributed hydrologic models to represent glacier dynamics. We
10 compare predicted variations in glacier extent, snow water equivalent and streamflow discharge made with the integrated model with satellite estimates of glacier area and terminus position, observed streamflow and snow water equivalent measurements over the period of 1980–2007. Simulations with the coupled hydrology-glacier model reduce the uncertainty in streamflow predictions. Our results suggested that on average, the
15 glacier melt contribution to the Bow River flow upstream of Lake Louise is about 30 % in summer. For warm and dry years, however, the glacier melt contribution can be as large as 50 % in August, whereas for cold years, it can be as small as 20 % and the timing of glacier melt signature can be delayed by a month.

1   Introduction

20 Glaciers in Western Canada are in a general state of recession (Moore et al., 2009) with losses in glacier area in the Canadian Southern Rocky Mountains of almost 15 % since 1985 (Bolch et al., 2010). The discharge from these rivers provides a crucial water resource to the large dry areas in Canada's Prairie Provinces (Schindler and Donahue, 2006).
25   In partially glacierized basins, melting of seasonal snow cover and glaciers in summer provides a natural storage buffer for precipitation that accumulates as snow in

winter. In the case of glaciers, this source is not depleted on an interannual basis, and in fact melt generally increases in warm dry periods, essentially providing a negative feedback to seasonal climate forcings (Fountain and Tangborn, 1985). Thus despite the fact that the glacier melt contribution to the flow of major rivers like the South Saskatchewan is modest on an annual basis, glacier melt can contribute substantially to late summer flows when water demand is highest (Comeau et al., 2009). As glaciers recede, there is an initial increase in streamflow due to higher melting, but over a longer time span the glacier melt contribution will eventually decrease due to reduction in glacier area. Stahl and Moore (2006) showed widespread negative trends in stream-flow within glacierized basins of British Columbia which they attributed to the effects of glacier retreat and suggested that in this region the time of increased streamflow has already passed (Stahl et al., 2008; Demuth et al., 2008). These observations broadly apply to the glacier sources of the South Saskatchewan River headwaters, however the normal pattern of initially increased summer flows is somewhat less apparent, possibly due to a concurrent multi-decade downward trend in winter precipitation and increased evapotranspiration (Schindler and Donahue, 2006).

Despite the risk posed by declining glaciers to water supply in the high mountain river systems, our ability to predict the runoff contribution from partially glacierized basins is limited. Modeling the effect of glacier changes on streamflow in such basins is complicated due to limited availability of high resolution gridded meteorological data and long term measurements of glaciological parameters. One approach that has been used to address these issues is to adapt models with a snow hydrology heritage, such as the Snowmelt Runoff Model (SRM; Martinec, 1975), HBV (Lindström et al., 1997; Bergström, 1976), SNOWMOD (Jain, 2001; Singh and Bengtsson, 2004) and apply them to estimate streamflow in river basins partially covered by glaciers and partially by seasonally ephemeral snow cover (see e.g., Singh and Bengtsson, 2004; Hock, 2003; Rees and Collins, 2006; Immerzeel et al., 2009 for applications). The disadvantage of these approaches is that the area of seasonal snow cover and glaciers either must be prescribed, or, in the case of glaciers, must be assumed to be fixed. Furthermore,

Title Page

Abstract | Introduction

Conclusions | References

Tables | Figures

◄ | ►

◄ | ►

Back | Close

Full Screen / Esc

Printer-friendly Version

Interactive Discussion

all of these models use temperature index snowmelt formulations, which require some calibration to current climate conditions. On the other hand, ice dynamic models with a range of complexities have been developed to predict long-term glacier response to climate variations (Le Meur and Vincent, 2003; Kessler et al., 2006; MacGregor et al.,
5   2000). Most of these models, however, are not linked to other hydrological processes such as evapotranspiration, surface runoff and baseflow which make their application to partially glacierized basins problematic.

Furthermore, knowledge of subglacial topography is not known for many mountain glaciers worldwide. Therefore, many modeling studies that have addressed the impact
10 of glacier changes on hydrology treat the glacier as static ice (e.g., Akhtar et al., 2008; Hagg et al., 2006) or update the glacier outlines periodically (e.g., once per decade) by applying a volume-area scaling relationship (Stahl et al., 2008). Such approaches, however, ignore the potentially important role of ice dynamics on future glacier changes and consequently on streamflow dynamics.

15 Jost et al. (2012) used a stand-alone glacier dynamics model to predict the evolution of glacier extent in time, and used this information to update the glacier extent in hydrologic model simulations. Their approach is much different than what we describe here (Sect. 2) – in particular, they treat glaciers as static ice masses that melt in place and, over time, lose volume. Using either prescribed (e.g., from satellite estimates)
20 or model-derived ice extent (from a glacier dynamic model), they update the glacier outlines once-per-decade. While this strategy is expedient and avoids the necessity of knowing or estimating subglacial topography, it does not account for changes in ice volume related to ice dynamics and its effect on glacier melt. The approach we describe instead explicitly couples a glacier dynamics component with a physically-based hydro-
25 logic model, which allows explicit simulation of the glacier mass and energy balance and dynamically adjusts the glaciated areas and volume depending on accumulation and ablation conditions at each (monthly) time steps of the glacier dynamics model. This approach also avoids the necessity of stopping and restarting the model simulation to update the ice extent.

Title Page

Abstract | Introduction

Conclusions | References

Tables | Figures

|◄ | ►|

◄ | ►

Back | Close

Full Screen / Esc

Printer-friendly Version

Interactive Discussion

CC BY

This fully integrated approach we describe herein avoids the inter-dependence of offline simulations from two models and allows the continuous prediction of glacier extent through time, at much shorter time step. This continuous simulation of glacier mass is critical for evaluating the effects of long-term deglaciation in the context watershed hydrology, where accurate simulation of glacier melt is necessary at inter and intra-annual timescales.

The objective of our study is to integrate a spatially distributed hydrologic model and a physically based distributed glacier dynamic model in order to assess streamflow response associated with glacier dynamics, and snow accumulation and ablation. We first describe our approach to coupling the Distributed Hydrology Soil Vegetation Model (DHSVM; Wigmosta et al., 1994) with the glacier dynamics model (Jarosch et al., 2013). We then test the ability of the integrated model to represent the effect of glacier dynamics on streamflow response in the partially glacierized Upper Bow River basin, Alberta.

2 Modeling approach

2.1 DHSVM

DHSVM, originally developed by Wigmosta et al. (1994) is a physically-based spatially distributed hydrology model. The model subdivides a watershed into uniform cells (typically with spatial resolution 10–150 m) to capture the spatial variability of the physical characteristics of the watershed at the Digital Elevation Model (DEM) scale (Storck et al., 1998). The main objective of the model is to simulate the spatial distribution of soil moisture, snow cover, evapotranspiration and runoff production over a range of spatial scales, at hourly to daily time scales. DHSVM uses a two-layer canopy representation for evapotranspiration (overstory and understory), a two-layer energy balance model for snow accumulation and melt, a multilayer unsaturated soil model and a saturated subsurface flow model (Storck et al., 1998). The two-layer energy and

mass balance approach to simulating snow accumulation and melt is similar to that described by Anderson (1968). The mass balance components represent snow accumulation/ablation, changes in snow water equivalent, and water yield from the snowpack (Wigmosta et al., 1994), while the energy balance components account for net radiation and sensible and latent heat transfers, as well as energy advected by rain, throughfall or drip (Storck, 2000). To run the model, input parameters are required for every grid cell in the watershed. These include meteorological observations such as precipitation, air temperature, wind, humidity and incoming short-wave and long-wave radiation (which, as a practical matter, are usually interpolated from (gridded) station data), and land surface characteristics such as vegetation, soils and digital elevation data. The distributed parameter approach allows the model to simulate not only the spatial distribution of soil moisture, snow cover, evapotranspiration and runoff but also to predict the overall streamflow response at watershed scale.

DHSVM has been successfully applied to a number of catchments in the western US and Canada to simulate the streamflow response of forested watersheds located in high-altitude areas (e.g., Storck et al., 1998; Bowling and Lettenmaier, 2001; Whitaker et al., 2003; Thyer et al., 2004). In more recent studies, DHSVM has been extended to account for glacier melt in the partially glacierized basins of the Western United States (Dickerson, 2009; Chennault, 2004). However, in these studies glaciers were represented as static deep snowpacks by specifying an initial amount of snow water equivalent in each pixel equal to the approximate depth of glacial ice (Dickerson, 2009). This approach could result in distortion of the parameters that control snow accumulation and glacier melt and consequently transient changes in glacier areas and their effect on streamflow.

2.2 Glacier flow model

The ice-flow model is based on the shallow ice approximation (SIA) (e.g., Greve and Blatter, 2009) and solves time-evolving and spatially-distributed balance equations for glacier mass and momentum. The vertically-integrated equation for the volume flux of ice is

$$q = -\frac{2A(\rho_{ice}g)^n \left|\nabla_{xy}S\right|^{n-1}}{n+2} H^{n+2}\nabla_{xy}S + v_B H \tag{1}$$

where $q = q_x \boldsymbol{i} + q_y \boldsymbol{j}$ is the two-dimensional ice flux vector ($m^2\,yr^{-1}$) and the right-hand side terms correspond to the flow contributions of creep and sliding respectively. In the foregoing equation, $A = 7.5738 \times 10^{-17}\,Pa^{-3}\,yr^{-1}$ and $n = 3$ are the coefficient and exponent of Glen's flow law for ice creep (Glenn, 1955), $\rho_{ice} = 900\,kg\,m^{-3}$ is the ice density, $g = 9.80\,m\,s^{-2}$ is the gravity acceleration, H is ice thickness, S is the ice surface elevation, and ∇_{xy} is the two-dimensional gradient operator. The basal sliding velocity is approximated by the Weertman sliding law (Weertman, 1957)

$$v_B = -C(\rho_{ice}g)^m H^m \left|\nabla_{xy}S\right|^{m-1}\nabla_{xy}S \tag{2}$$

where C is a coefficient that controls the sliding rate, and m is an exponent (e.g., Weertman, 1957; Cuffey and Paterson, 2010).

Equation (1) gives the momentum balance equation for slow shear flow and, for constant ρ_{ice}, the continuity equation

$$\frac{\partial H}{\partial t} = -\nabla_{xy}q + \frac{\rho_{ice}}{\rho_w}b_n \tag{3}$$

is equivalent to the mass balance equation where b_n is the water-equivalent mass balance rate ($m\,yr^{-1}$). By defining the nonlinear momentum diffusivity as

$$D(H, S_{xy}) = \frac{2A(\rho_{ice}g)^n \left|\nabla_{xy}S\right|^{n-1}}{n+2}H^{n+2} + C(\rho_{ice}g)^m \left|\nabla S_{xy}\right|^{m-1} H^m, \tag{4}$$

5019

and noting that $H = S - B$ where B is the bed surface topography (assumed to be fixed), it follows that $\partial H/\partial t = \partial S/\partial t$ and Eq. (3) leads to a nonlinear diffusion equation of the form $\partial S/\partial t = \nabla_{xy} \cdot (D\nabla_{xy}S) + \rho_{ice}b_n/\rho_w$. We solve this equation numerically using a semi-implicit finite-difference scheme that is similar in spirit to the standard
5 Crank–Nicolson method (e.g., Press et al., 2007) but which can optionally exploit the possibility of being "super-implicit" in order to ensure stability when time steps are large (Hindmarsh, 2001). The essence of our modeling approach is a standard one in glaciology and has been used for simulating the dynamics of ice sheet and ice caps (e.g., Huybrechts, 1992; Marshall et al., 2000; Hindmarsh, and Payne, 1996) and of moun-
10 tain glaciers (e.g., Le Meur and Vincent, 2003; Plummer and Phillips, 2003; Kessler et al., 2006).

In regions of extreme topography, conventional SIA ice-flow models can yield *negative* ice thicknesses, unphysical behavior that leads to violations of the mass conservation principle upon which Eq. (3) is based. This problem can be addressed by
15 introducing flux limiters when the momentum diffusivity Eq. (4) is calculated (Jarosch et al., 2013). Our scheme exploits flux limiters by upwinding ice thickness H in Eq. (4) whereas the scheme proposed by Jarosch et al. (2013) applies upwinding to both H and $\nabla_{xy}S$ and is somewhat more robust than ours. In all other respects the two approaches are comparable.

20 ## 2.3 Model integration

In order to account for the glacier melt contribution to streamflow from changes in glacier area or volume, the glacier dynamic model was fully merged into the DHSVM modeling framework as shown in Fig. 1. To predict the present-day ice thickness distribution, the glacier flow model requires subglacial topography and net annual mass
25 balance (Fig. 1a). On average, snow accumulates in areas where the net annual mass balance is positive (i.e., above the equilibrium line). As snow accumulates at higher elevations, the glacier dynamic model transports the ice mass downhill to the areas where the mass balance is negative. By running the model for a long enough spinup

period, the ablation area eventually expands so that annual volume of accumulated and ablated ice are equal and a steady state is reached. We used the average ice thickness distribution from the spinup simulation to initialize the integrated model.

In the integrated model, we modified the DHSVM surface energy balance snow model to estimate glacier mass balance using sub-daily forcing data (Fig. 1b). Specifically, the two-layer full energy and mass balance snow model was modified to add an ice layer in order to account for glacier ice melt (Fig. 1c). To define total ice volume for the ice layer in the integrated model, the ice layer was initialized with the present-day ice thickness estimated at the end of the glacier model spin-up time period. As shown in Fig. 1c, for each glacier cell the upper two snow layers overlie a bottom layer of glacier ice. When the snow has completely melted, the ice layer becomes exposed and continues to thin by melting at a rate determined using a modification of the energy balance approach incorporated in DHSVM. The ice water equivalent (IWE) (mw.e.) of the ice layer is therefore updated at sub-daily time steps only through ice melt. Any snow that falls on a glacier cell increases the snow depth of the upper snow layers. The amount of accumulated SWE greater than 5 mw.e. on the glacier surfaces which is not melted completely at the end of the melting season is added to IWE and subtracted from the SWE.

The net monthly mass balance is determined from the change in storage states of SWE and IWE during each month as follows:

$$b_n = \Delta\text{IWE} + \Delta\text{SWE} \tag{5}$$

where ΔIWE (mw.e.) is the monthly change in the ice layer as a result of ice melt and ΔSWE (mw.e.) is the monthly change in snow water equivalence through snow accumulation and snow melt in a given month.

The ice dynamics are computed at a monthly time step in the integrated model. During the glacier model run, the surface topography is updated as a function of net monthly mass balance and the ice flux in and out of the grid cell. The ice thickness is updated as result of changes in the glacier surface topography as follows:

5021

$$h(i,j,t+\text{dt}) = \begin{cases} 0, S(i,j,t) \leq B(i,j,t) \\ S(i,j,t) - B(i,j,t), S(i,j,t) > B(i,j,t) \end{cases} \tag{6}$$

where $S(i,j,t)$ is the surface elevation (m a.s.l.) and $B(i,j,t)$ is the bed elevation (m a.s.l.) at the ith and jth grid cell. dt is the monthly time step in years. In the glacier flow model, h is the total thickness of both snow and ice layers. Any snow accumulation in the ice-free areas at the end of the melting season will also increase the surface elevation which may lead to errors in the estimation of ice extent. To avoid this condition, the glacier area is only allowed to grow or retreat into the area of its historical extent.

At the end of the each one-month time step of the glacier dynamics model, the thickness of the IWE layer in DHSVM is adjusted as result of glacier movement as follows:

$$\text{IWE}_t(i,j,t+\text{dt}) = (S(i,j,t) - (S(i,j,t-\text{dt}) + b_n(i,j,t))) \times \frac{\rho_{\text{ice}}}{\rho_w} \tag{7}$$

where IWE_t is the amount of ice flux in or out of grid cell, $S(i,j,t)$ is the surface elevation at the current step and $S(i,j,t-\text{dt})$ is the surface elevation at the previous time step of the glacier flow model.

3 Case study: Upper Bow River basin

3.1 Study site description and data

The Bow River originates in the Canadian Rocky Mountains and is a major tributary to the South Saskatchewan River, which flows eastward across southern Alberta (Fig. 2). The Upper Bow River has a drainage area of $422\,\text{km}^2$ above the Lake Louise town site with elevations ranging from 1200 to 3300 m. The mean annual precipitation at the Lake Louise weather station is about 600 mm but is thought to be as high as 1200 mm at

Title Page

Abstract | Introduction

Conclusions | References

Tables | Figures

|◀ | ▶|

◀ | ▶

Back | Close

Full Screen / Esc

Printer-friendly Version

Interactive Discussion

higher elevations, mostly in the form of snow. Mean summer (June–August) and winter (December–March) air temperatures are 7 and −12 °C, respectively. The hydrological regime of the Upper Bow River is strongly influenced by glacier melt and snowmelt with the maximum monthly discharge in summer (June–August) and the minimum monthly

5 discharge in February and March.

Because the boundaries of the glaciers are not coincident with the river/stream basin boundaries, we ran the coupled glacio-hydrological model for a 200 × 200 m resolution rectangular subset (191 rows and 179 columns) with total area of 1367 km^2 as shown in Fig. 2. Glacier cover derived from Landsat Thematic Mapper scenes (see Appendix A

10 for more detail on glacier mapping techniques) showed that glacier cover in the study domain has declined from 150 km^2 in 1986 to 126 km^2 in 2011 representing 9 % of the total study domain (Fig. 3). For routing of streamflow to the outlet of the basin, the drainage network used in the model was however only derived for pixels within the drainage basin (Fig. 4a). The 90 m resolution SRTM DEM (the seamless dataset with

15 filled voids available from the Consultative Group for International Agriculture Research Consortium for Spatial Information (CGIAR-CSI) via http://srtm.csi.cgiar.org/ is used in the present study) as shown in Fig. 4b was used to delineate the basin boundary at the gauge station above Lake Louise. The land-cover information based on Landsat imagery from 1990 derived by Agriculture and Agri-Food Canada was used with a total

20 of seven land-cover classes in the study domain (Fig. 4c). Areas that are currently glacierized were represented as a separate class in the land-cover data set based on glacier outlines delineated using the oldest available Landsat image (8 August 1986). The soil class map and soil physical properties for the study area were taken from the Soil Landscapes of Canada database (Fig. 4d). Soil properties similar to those of bare

25 rock class were used for the glacierized areas. Soil depth information was derived from the DEM (Fig. 4e) based on local slope (determined from the DEM), upstream source area, and elevation.

The climate forcing data required by the coupled model are precipitation, temperature, wind speed, downward short- and long-wave radiation, and relative humidity. In

the glacierized portion of the basin, determining these climate variables is difficult due to various controlling factors such as the influence of orography on precipitation, shadowing effects, and topographic aspect variations. In DHSVM, the climate data records at specific meteorological stations are distributed to each grid cell in the model through interpolation schemes using temperature and precipitation elevation lapse rates, or through gridded temperature and precipitation maps (Wigmosta et al., 1994). Climate daily data such as minimum, maximum, wind speed and precipitation are available at the Lake Louise station (elevation: 1524 m) for time period of 1915–2007. Because of significant spatial and temporal variability in precipitation and significant missing records at the climate station, we therefore used 1 km downscaled North American Regional Reanalysis (NARR) daily precipitation data for the 1979–2007 time period (for a detailed description of the downscaling methodology, see Jarosch et al., 2012). To run the model at 3-hourly time step, the daily 1 km NARR precipitation data extracted at the location of Lake Louise station were temporally disaggregated by equally apportioning days to 3-hourly intervals (Fig. 2). In addition to precipitation, temperature, downward solar and longwave radiation data were derived at 3-hourly interval from the daily temperature range and daily total precipitation using methods described in Nijssen et al. (2001). We selected 1979–2007 as our period of analysis.

Daily streamflow data from the gauge station located near Lake Louise were used to evaluate the modeling results. The Lake Louise gauge station, which is operated by Water Survey of Canada (WSC), was established in 1910 and continuous flow data are available until 1986. From 1987 on, stream discharge was only measured for the high flow months (May to October). In addition to measured streamflow data, snow water equivalent (SWE) data from snow course measurements were also available for the model simulation time periods for two different locations within the basin (Fig. 2).

The glacier component of the coupled model requires subglacial topography. Bed surface topography was estimated using DEM data and the ice mask in order to algorithmically remove existing ice cover following the methodology described in Clarke et al. (2012) (Fig. 4f).

3.2 Integrated model implementation

To initialize the coupled glacio-hydrological model with the glacier extent and ice thickness that exist under present climatic conditions, the stand-alone glacier dynamic model was run forward in time for 1000 yr to allow the glaciers to reach a steady state condition for which the simulated glacier extent matched the glacier terminus positions that have been identified from oldest available Landsat image of 1986 (Sect. 3.1). The input to the glacier dynamic model includes bed surface topography and a steady but spatially-varying mass balance that corresponds to the present-day net average annual mass balance. For this spin-up run, we first quantified the net annual mass balance field using a simple temperature index model where annual ablation is calculated using 1 km downscaled NARR daily precipitation data and 200 m downscaled NARR temperature data for the period 1979–2008. We used a degree day factor (DDF) of $3.9\,\text{mm}\,\text{d}^{-1}\,^\circ\text{C}^{-1}$ based on Radić and Hock (2011) for Peyto Glacier located in the study domain (Fig. 2). The annual snow accumulation was calculated from the sum of daily solid precipitation assuming that precipitation fell as snow if daily average air temperature was below $0\,^\circ\text{C}$. Using the DDF of $3.9\,\text{mm}\,\text{d}^{-1}\,^\circ\text{C}^{-1}$, negative mass balance distribution of most glaciers was predicted which is generally consistent with the observed current glacier retreat in this region but is not be representative of the climate condition that allow for glacier growth (Fig. 5). We therefore tested a range of increases relative to the computed 1979–2008 average net annual mass balance until the best agreement between observed and predicted Eq. (1) glacier outlines, and Eq. (2) basin-average percentage glacier cover was achieved. The increase in mass balance was only applied to the grid cell values inside the observed glacier outlines.

Figure 6 shows examples of computed glacier growth for the Bow River basin with no change in mass balance outside the glacier boundary but with increases in mass balance for glacierized areas within the basin ranging from 1.3 to 1.7 m. Comparing the simulated glacier extents at the end of model spin up time period (1000 yr) with observed glacier outlines shows that an increase of 1.6 m above the 1979–2008 averaged

Title Page

Abstract | Introduction

Conclusions | References

Tables | Figures

◄ | ►►|

◄ | ►

Back | Close

Full Screen / Esc

Printer-friendly Version

Interactive Discussion

mass balance within the glacierized portion of the basin reproduces the overall extent and terminus positions for many glaciers quite well (Fig. 6c). At the end of the glacier model spin-up period, the simulated percent glacier cover areas for the study domain is about 9 %, whereas the total percent glacier cover from the 1986 Landsat image is

5 12 %. The 3 % underestimation of glacier cover is due in part to the use of the 1979–2008 averaged net mass balance which reflects the condition of current negative mass balance. Our sensitivity analysis shows that an increase of 1.7 m in the mass balance of glacierized areas produces a good match for the retreated glaciers but leads to advances for other glaciers (Fig. 6d). Using the 1979–2008 mass balance distribution,

10 augmented by 1.6 m within glacierized areas, as a constant forcing, requires about 650 yr for the glacier to reach a steady state (Fig. 7).

After the spin up run was completed, the steady state glacier geometry derived from the glacier flow model was used to calculate the ice thickness distribution using Eq. (2) to initialize the coupled model. In the integrated model, glacier ice dynamics are com-

15 puted at a monthly time interval where the glacier mass balance (net of accumulation and melt), is calculated using Eq. (1) at sub-daily times. As described in Sect. 2.3, the ice thickness distribution and glacier extent at the end of each month are updated using Eqs. (6) and (7).

3.3 Integrated model calibration and evaluation

20 The Upper Bow River basin was simulated at 200 m resolution at a 3-hourly time step using the coupled glacio-hydrologic model. The coupled model was run for the time period 1979–2007 with a one year spin-up. The simulation period was divided into calibration and verification periods, with odd-year data used for calibrating the parameters of DHSVM, and even-year data for verifying them. The reason for using odd and even

25 years to represent calibration and verification periods rather than the more traditional approach of setting aside different periods of record is to ensure that the statistical properties of the calibration and verification periods are similar. Model performance in predicting streamflow, snow accumulation and melt patterns, and changes in glacier

cover for both calibration and validation time periods was evaluated through compari-
son with observed daily streamflow, SWE measurements, MODIS snow cover data and
Landsat-derived ice cover.

The model performance in predicting streamflow was also evaluated using the Nash–
Sutcliffe efficiency coefficient (NS) (Nash and Sutcliffe, 1970) as:

$$NS = 1 - \frac{\sum \left[Q_s(i) - Q_o(i) \right]^2}{\sum \left[Q_o(i) - \overline{Q_o} \right]^2} \qquad (8)$$

where Q_s is the simulated discharge at month or day i, Q_o is the monthly observed
discharge, and $\overline{Q_o}$ is the mean of Q_o. The case of NS = 1 represents perfect agreement
between simulated and observed discharge, while a NS value less than 0 signifies that
the mean is a better estimate than the model data.

Because of the distributed nature of both the glacier and DHSVM models, the cou-
pled glacio-hydrologic model is computationally-intensive. Key calibration parameters
as summarized in the Table 1 were therefore identified and then one-at-a-time searches
were performed to optimize the calibrated parameters. Calibration was performed to
optimize the model's soil parameters such as lateral hydraulic conductivity and rate
of exponential decrease in hydraulic conductivity with depth (Table 1). This calibration
resulted in increasing the low winter flow and decreasing the higher peaks in summer.

Furthermore, the sensitivity analysis showed that snow albedo is the most critical pa-
rameter affecting snow accumulation and melt. In DHSVM, the snow albedo curves are
calculated separately for accumulation and melt following the approach of Laramie and
Schaake (1972). DHSVM uses the maximum albedo value even after a light snowfall
event, which has been shown to cause the snow albedo to be overestimated (Whitaker
et al., 2003). We adjusted the snow albedo curves by lowering the albedo for both
accumulation and melt. Figure 8 shows comparisons of snow course data within the
Bow River basin, which are measured at the lower elevation Bow Summit, and higher
elevation Katherine Lake sites with the simulated SWE for the period of 1980–2007

**Modeling the effect
of glacier recession
on streamflow
response**

B. S. Naz et al.

Title Page

Abstract	Introduction
Conclusions	References
Tables	Figures

|◄ | ►|
◄ | ►

| Back | Close |

Full Screen / Esc

Printer-friendly Version

Interactive Discussion

at the same locations. Adjustment of the albedo curve was effective in correcting the over prediction of the SWE for some years at the Katherine Lake site. The albedo adjustment also improved the timing of the simulated snow accumulation and ablation for both sites. The snow course data at the lower elevation Bow summit site are accurately reproduced by the model (Fig. 8a), but the model overestimates the maximum SWE at the Katherine Lake site for a few years where measured SWE is available for the winter months (Fig. 8b). For many other years, the maximum SWE data are not available for this site.

The coupled glacio-hydrologic model performance was further evaluated for predicting area-averaged ice-cover at the end of the melt season in each year by comparing with Landsat-derived ice extent available for 7 scenes in the period 1986–2007. Our initial results showed accelerated decrease in predicted ice cover extent over time when compared to observed extents partly due to the warmer temperature at the station location which may not be representative of the higher elevations on the glacier. For this reason, sensitivity of the integrated model in predicting glaciers extent was evaluated using different temperature and precipitation lapse rates through comparison of area-average predicted ice cover extent with satellite-derived ice cover. Based on this analysis, temperature and precipitation lapse rates of $-0.0070\,^\circ\mathrm{C}\,\mathrm{m}^{-1}$ and $0.0002\,\mathrm{mm}^{-1}$ were selected, respectively (Table 1).

To test the validity of our selected precipitation and temperature lapse rates and the model performance in predicating spatial variability of snow/ice accumulation and ablation, we used observations of mean annual specific mass balance for the Peyto glacier over the period of 1980–2007 (Demuth et al., 2009; WGMS, 2010) to compare with our model-predicted glacier mass balance. Area average specific mass balance in coupled model is computed as follows:

$$\frac{\sum_{i=1}^{n} b_i}{\sum_{i=1}^{n} N_i}, \tag{9}$$

where b_i are mass balance values and N_i are the number of observation ($i = 1\ldots n$) within glacier extent of study domain. The mass balance values b_i are calculated using Eq. (5). By running the model for 1980–2007, we obtained mean annual mass balance of -778 m w.e. for the Peyto glacier which agreed well with its observed mass balance of -774 m w.e. averaged over the same period. The modeled cumulative specific mass balance for Peyto and Bow Glaciers are shown in Fig. 9, which compare well with the observed cumulative mass balance for the same period, although modeled mass balance for the Bow Glacier became slightly more negative than Peyto Glacier since 2000. The missing values of measured mass balance values for year 1990 and 1991 for Peyto Glacier were filled in with mean annual mass balance value over the entire period.

Model performance in simulating streamflow was assessed by comparing simulated with observed daily streamflow for both calibration and validation years. The daily NS value for calibration years was 0.70 while for the validation years, it was 0.73 (Table 2). The calibrated model shows overall good fit to the observed hydrographs for most years except the late summer flow in many years was underpredicted (Fig. 10). The underprediction of late summer flow is associated with the underestimated simulated glacier extent, particularly for retreating glaciers where glacier melt contribution in late summer is generally higher. With the glacier model included, the distributed hydrologic model was better able to capture the seasonal cycle of annual discharge, particularly the late summer flow when the glacier melt contribution is highest. Without glaciers represented in the model, the daily NS value decreased from 0.70 to 0.57 and 0.73 to 0.65 for calibration and validation time periods, respectively (Table 2).

3.4 Role of glacier dynamics on ice cover changes and streamflow response

Comparisons of the predicted ice cover at the end of the melt season each year with the Landsat-derived ice cover are shown in Fig. 11. As discussed in Sect. 3.2, underestimation of glacier extent by the glacier dynamics model at the end of the spin-up time period is evident near the beginning of the simulation, but the modeled glacier area

Title Page

Abstract | Introduction

Conclusions | References

Tables | Figures

◄ | ►|

◄ | ►

Back | Close

Full Screen / Esc

compares well with the observed glacier cover in recent years. This also illustrates that model is better able to capture the variations in glacier area through mass balance-elevation feedback by transporting ice to lower elevation under transient mass balance conditions.

⁵   The effect of glacier melt changes on streamflow dynamics was explored by comparing the difference in mean annual daily simulated and observed hydrographs; and glacier melt contribution for the period 1980–2007. The glacier melt contribution to discharge was calculated form the difference in streamflow with and without glacier simulation. The mean annual daily ice melt contribution varied between 5 and 30 %
¹⁰ between July–September with the highest contribution (30 %) occurring in late August (Fig. 12a). Figure 12 also compares simulated streamflow with and without the presence of glacier and the relative contribution of glacier melt for the warmest (1998) and coldest (1999) years. The warmest and coldest years were selected based on the maximum and minimum number of positive degree days, respectively, during the sim-
¹⁵ ulation period. In the coldest year (1999), the glacier melt started later in July while the highest contribution to annual flow occurred in late August (20 %) (Fig. 12b). For the warm year 1998, the glacier melt started early in June with more than 40 % contribution throughout late summer (July–September), and in August glaciers provided up to 58 % of discharge (Fig. 12c).
²⁰   Trend analysis was performed using the Mann–Kendall test (Mann, 1945; Kendall and Gibbons, 1962) and Sen's slope estimator (Sen, 1968). The Mann–Kendall test is a non-parametric test for monotonic trend that assumes independent, identically distributed data (Hirsch and Slack, 1984; Helsel and Hirsch, 1988). The Sen's slope estimator calculates the slope using the median of all pairwise slopes in the data set. This
²⁵ analysis showed decreasing trends in both simulated summer ($-0.10\,\mathrm{mm\,yr^{-1}}$) and total annual ($-0.14\,\mathrm{mm\,yr^{-1}}$) streamflow for the period 1980–2007 (Table 3); the trends however are not statistically significant. Similarly, statically significant trends were not identified in annual and summer glacier melt, but both exhibit consistent upward trend direction over the simulation period. The downward trends direction in streamflow might

Title Page

Abstract   Introduction

Conclusions   References

Tables   Figures

◄   ►

◄   ►

Back   Close

Full Screen / Esc

Printer-friendly Version

Interactive Discussion

be attributable to a decreasing trend in annual precipitation (not statistically significant (p value of 0.49) and/or a $\sim 15\%$ decrease in simulated glacier cover. On the other hand, the increasing trends direction in glacier melt contribution to total runoff might be associated with statistically significant upward trends in positive degree days of 0.38 pdd yr^{-1} and mean annual temperature (0.08 °C yr^{-1}); these trends however may have little impact on annual and summer streamflow in a watershed of this size relative to changes in precipitation and evapotranspiration.

4 Discussion

Simulations from the coupled glacio-hydrological model demonstrate that the representation of the influences of dynamic processes of glacier accumulation, ablation, and ice flow, in a distributed hydrology model, improves the prediction of streamflow response as compared with observations. However, the model tends to produce systematic underestimates of discharge particularly in late summer which is attributed in part to the underestimation of initial ice cover used to initialize the integrated model (Fig. 12a). The effect of underestimation of initial glacier cover on streamflow variability, however, is decreased later in the simulation period due to the mass balance-elevation feedback in the glacier flow model which transports ice in underestimated glacier areas in early summer, providing more glacier melt in the late summer.

The greatest sources of errors in estimating the initial ice thickness distribution are associated with uncertainty in the mass balance and bed topography (Clarke et al., 2012). Because there are insufficient data to validate the subglacial bed topography, we assume that it is correct and only applied adjustments to the mass balance fields that forced the glacier model to grow glaciers in the glacierized parts of the study domain. The adjustment (Sect. 3.2) was made by increasing the mean annual mass balance in the glacierized areas that would responsible for glacier growth and realistically reproduce the shapes and terminus position of the glaciers under modern climate condition. In this regard, the glacier outlines derived from the 1986 Landsat image were

the only indicator of how well the model reproduced the current glacier shapes and ice thickness distribution. The terminus positions of small glaciers, however, were not reproduced very well, causing a small underestimation in the simulated glacier cover at the end of glacier model spin-up run. Despite the increases in the spatial distribu-
⁵ tion of mean annual mass, the underestimation by the model of glacier cover might be attributed to the bias in the NARR data reported by other studies for the Canadian Rockies region (Jarosch et al., 2012). Another important source of uncertainty in esti-mating the initial glacier mass balance information for the glacier model is the assumed value for the degree day factor, taken as $3.9\,\mathrm{mm\,d^{-1}\,{}^\circ C^{-1}}$ in our study. This estimate,
¹⁰ which is based on other studies for Peyto Glacier (Radic and Hock, 2011) may not be representative of the glaciers in the Bow river headwaters.

Despite the uncertainty in initial ice thickness and ice cover, incorporating the glacier dynamics model into DHSVM clearly improved Bow River streamflow predictions. With-out incorporating the glacier area changes through glacier flow in model calibration, it
¹⁵ is difficult to identify uncertainties in mass balance because inaccurate glacier mass balance fields do a worse job in simulating glacier terminus positions as illustrated in Fig. 6, but may produce better model performance in terms of streamflow prediction (Jost et al., 2012; Stahl et al., 2008). Our results indicate that comparing the predicted glacier cover with satellite-derived ice cover eliminates the need for incorporating mass
²⁰ balance data in the calibration process as has been done in other studies (Schaefli and Huss, 2011; Konz and Seibert, 2010; Stahl et al., 2008). Our modeling approach not only allows direct consideration of the effects of changes in climatic conditions on glacier extents, but also helpful to evaluate uncertainty in predicting glacier melt con-tribution to discharge in remote glacierized basins worldwide where measurements of
²⁵ glacier mass balance are not available.

5 Conclusions

We have documented the integration of a spatially distributed glacier dynamics model with the Distributed Hydrology Soil Vegetation Model (DHSVM) and used the integrated model to investigate the effect of glacier recession on streamflow over the last three decades in the partially glacierized Upper Bow River basin, Alberta, Canada. Despite uncertainty in our initial ice thickness distribution and glacier extent estimate, the integrated model was better able to capture how climate variations cause changes in glacier cover and streamflow dynamics. Thus the model more accurately predicts the glacier melt contribution to streamflow when compared with model simulations without glaciers or simulations that consider ice to be static. Using the integrated model to simulate glacier effects on streamflow variations over the last three decades, we have shown that:

1. On average, the glacier melt contribution to Bow River streamflow is about 30 % in summer. This contribution however can increase up to 50 % in August for warm and dry years, whereas in cold years, the August glacier melt contribution can be as small as 20 %, and is delayed by about a month.

2. Despite the simulated 15 % decrease in glacier cover over the period of 1980–2007, no statistically significant trends were observed in annual and summer runoff. The downward trend direction in summer and total streamflow, however, might be associated with a combined effect of decreases in glacier cover and precipitation.

3. Our results showed that glaciers in the Upper Bow River basin are still in a phase of enhanced contribution to the late summer flow as evidenced by the upward trend in glacier melt contribution to streamflow and therefore, glaciers in this basin have not yet reached a limiting volume despite the decline in glacier area.

Our findings illustrate that under an extreme future climate condition in which all glaciers disappear, late summer discharge could be reduced substantially. These

⏮ | ⏭

◀ | ▶

Back | Close

Full Screen / Esc

Printer-friendly Version

Interactive Discussion

changes will have important implications for water availability in dry- and low-flow seasons in future decades, on both local and regional scales.

Appendix A

Glacier mapping methodology

The suitability of satellite imagery for estimation of glacier extent depends on cloud cover, the date of acquisition, and the effects of seasonal snow. For this study we selected (nearly) cloud-free scenes that were acquired late in the dry season (August or September) when seasonal snow was assumed to be at a minimum. We used imagery from two sensors: Landsat 2 Multispectral Scanner (MSS) and Landsat 5 Thematic Mapper (TM). Although the Landsat satellites have relatively short repeat cycles (ex: 16 days for TM), the presence of cloud-cover in mountain environments and the seasonal limitation make it difficult to acquire multiple images for any one year.

We selected ten scenes for analysis from the following years: 1986, 1991, 1994, 1998, 2001, 2004, 2007, 2009 and 2011 (Table A1). All scenes were downloaded from the United States Geological Survey (USGS) Earth Resources Observation and **S**cience (EROS) Center, and were already orthorectified and projected. For all Landsat scenes used in this study, the elevation source for orthorectification was the Global Land Survey (GLS) 2000 dataset. All scenes were projected (by EROS) to the North American Datum (NAD) 1983 coordinate system, zone 11N.

We converted Landsat TM digital numbers (DN) to top-of-atmosphere (TOA) radiance using preprocessing tools in ENVI v.4.8. We then converted top-of-atmosphere radiance to surface reflectance using the atmospheric correction model Second Simulation of a Satellite Signal in the Solar Spectrum (6S; http://6s.ltdri.org/) (Vermote et al., 1997). For each correction, we set the target altitude to 2.5 km a.s.l., which is approximately the lowest glacier terminus elevation in the basin.

Similar to a previous study in this region (Bolch et al., 2010), we used the ratio of Landsat band 3 to band 5 to map glaciers:

$$b3/b5 = \frac{\rho_{VIS}}{\rho_{NIR}} \tag{A1}$$

where ρ_{VIS} is the reflectance in the visible part of the electromagnetic spectrum (specifically Band 3 for Landsat TM) and ρ_{NIR} is the reflectance in the near-infrared portion of the electromagnetic spectrum (specifically Band 5 for Landsat TM). Paul et al. (2007) found that this method worked well for mapping ice in shadows, although it tends to misclassify water bodies. We created an elevation mask to remove water bodies below 2000 m.

The ratio was computed in ENVI using bands that had been atmospherically corrected. We used GIS to reclassify the resulting calculation into glacier and non-glacier. Next, reclassified rasters were converted to polygons using GIS. Similar to other studies (e.g., Bolch et al., 2010; Racoviteanu et al., 2008), we deleted patches of snow and ice that were smaller than 0.1 km^2. Finally, obvious mapping errors, such as lakes above the 2000 m elevation mask, were deleted.

References

Akhtar, M., Ahmad, N., and Booij, M.: The impact of climate change on the water resources of Hindukush–Karakorum–Himalaya region under different glacier coverage scenarios, J. Hydrol., 355, 148–163, 2008.

Anderson, E. A.: Development and testing of snow pack energy balance equations, Water Resour. Res., 4, 19–37, 1968.

Bergström, S.: Development and application of a conceptual runoff model for Scandinavian catchments, SMHI, Report No. RHO 7, Norrköping, 134 pp., 1976.

Full Screen / Esc

Printer-friendly Version

Interactive Discussion

Bolch, T., Menounos, B., and Wheate, R.: Landsat-based inventory of glaciers in western Canada, 1985–2005, Remote Sens. Environ., 114, 127–137, 2010.

Bowling, L. C. and Lettenmaier, D. P.: The effects of forest roads and harvest on catchment hydrology in a mountainous maritime environment, Water Sci. Appl., 2, 145–164, 2001.

Chennault, J.: Modeling the contributions of glacial meltwater to streamflow in Thunder Creek, North Cascades National Park, Washington, Master Thesis, Western Washington University, USA, 78 pp., 2004.

Clarke, G. K., Anslow, F. S., Jarosch, A. H., Radic, V., Menounos, B., Bolch, T., and Berthier, E.: Ice volume and subglacial topography for western Canadian glaciers from mass balance fields, thinning rates, and a bed stress model, J. Climate, doi:10.1175/JCLI-D-12-00513.1, in press, 2012.

Comeau, L. E. L., Pietroniro, A., and Demuth, M. N.: Glacier contribution to the north and south saskatchewan rivers, Hydrol. Process., 23, 2640–2653, 2009.

Cuffey, K. M. and Paterson, W. S. B.: The physics of glaciers, Academic Press, Amsterdam, 2010.

Demuth, M., Pinard, V., Pietroniro, A., Luckman, B., Hopkinson, C., Dornes, P., and Comeau, L.: Recent and past-century variations in the glacier resources of the Canadian Rocky Mountains: Nelson River system, Terra Glacialis, 11, 27–52, 2008.

Demuth, M., Sekerka, J., and Bertollo, S.: Glacier Mass Balance Observations for Peyto Glacier, Alberta, Canada (updated to 2007), Spatially Referenced Data Set Contribution to the National Glacier-Climate Observing System, State and Evolution of Canada's Glaciers, available at: http://pathways.geosemantica.net/, Geological Survey of Canada, Ottawa, 2009.

Dickerson, S. E.: Modeling the effects of climate change forecasts on streamflow in the Nooksack River basin, Masters thesis, Department of Geology, Western Washington University, USA, 2009.

Flowers, G. E. and Clarke, G. K. C.: A multicomponent coupled model of glacier hydrology: 1. Theory and synthetic examples, J. Geophys. Res., 107, 2287, doi:10.1029/2001JB001122, 2002.

Fountain, A. G. and Tangborn, W. V.: The effect of glaciers on streamflow variations, Water Resour. Res., 21, 579–586, doi:10.1029/WR021i004p00579, 1985.

Glen, J. W.: The creep of polycrystalline ice, P. Roy. Soc. Lond. A, 228, 519–538, 1955.

Greve, R. and Blatter, H.: Dynamics of ice sheets and glaciers, Springer, Dordrecht, Netherlands, 77–83, 2009.

Title Page

Abstract | Introduction

Conclusions | References

Tables | Figures

|◄ | ►|

◄ | ►

Back | Close

Full Screen / Esc

Printer-friendly Version

Interactive Discussion

Hagg, W., Braun, L., Weber, M., and Becht, M.: Runoff modelling in glacierized Central Asian catchments for present-day and future climate, Nord. Hydrol., 37, 93–105, 2006.

Hall, D. K., Riggs, G. A., and Salomonson, V. V.: Development of methods for mapping global snow cover using moderate resolution imaging spectroradiometer data, Remote Sens. Environ., 54, 127–140, 1995.

Helsel, D. R. and Hirsch, R. M.: "Applicability of the t-test for detecting trends in water quality variables", by Montgomery, R. H. and Loftis, J. C., J. Am. Water Resour. Assoc., 24, 201–204, 1988.

Hindmarsh, R. C. A.: Notes on basic glaciological computational methods and algorithms, in: Continuum Mechanics and Applications in Geophysics and the Environment, edited by: Straughan, B., Greve, R., Ehrentraut, H., and Wang, Y., Springer-Verlag, Berlin, 222–249, 2001.

Hindmarsh, R. C. A. and Payne, A. J.: Time-step limits for stable solutions of the ice-sheet equation, Ann. Glaciol., 23, 74–85, 1996.

Hirsch, R. M. and Slack, J. R.: A nonparametric trend test for seasonal data with serial dependence, Water Resour. Res., 20, 727–732, 1984.

Hock, R.: Temperature index melt modelling in mountain areas, J. Hydrol., 282, 104–115, 2003.

Huybrechts, P.: The Antarctic ice sheet and environmental change: a three-dimensional modelling study, Ph.D thesis, Vrije Universiteit of Brussel, Germany, 1992.

Immerzeel, W., Droogers, P., De Jong, S., and Bierkens, M.: Large-scale monitoring of snow cover and runoff simulation in Himalayan river basins using remote sensing, Remote Sens. Environ., 113, 40–49, 2009.

Jain, S.: Snowmelt Runoff Modeling and Sedimentation Studies in Satluj Basin using Remote Sensing and GIS, Ph.D. thesis, University of Roorkee, India, 2001.

Jansson, P., Hock, R., and Schneider, T.: The concept of glacier storage: a review, J. Hydrol., 282, 116–129, 2003.

Jarosch, A. H., Anslow, F. S. and Clarke, G. K. C.: High-resolution precipitation and temperature downscaling for glacier models, Clim. Dynam., 38, 391–409, doi:10.1007/s00382-010-0949-1, 2012.

Jarosch, A. H., Schoof, C. G., and Anslow, F. S.: Restoring mass conservation to shallow ice flow models over complex terrain, The Cryosphere, 7, 229–240, doi:10.5194/tc-7-229-2013, 2013.

Modeling the effect of glacier recession on streamflow response

B. S. Naz et al.

Title Page

Abstract | Introduction

Conclusions | References

Tables | Figures

◀ | ▶

◀ | ▶

Back | Close

Full Screen / Esc

Printer-friendly Version

Interactive Discussion

Jost, G., Moore, R. D., Menounos, B., and Wheate, R.: Quantifying the contribution of glacier runoff to streamflow in the upper Columbia River Basin, Canada, Hydrol. Earth Syst. Sci., 16, 849–860, doi:10.5194/hess-16-849-2012, 2012.

Kendall, M. and Gibbons, J. D.: Rank Correlation Methods, Edward Arnold, A division of Hodder & Stoughton, A Charles Griffin title, London, 29–50, 1990.

Kessler, M. A., Anderson, R. S., and Stock, G. M.: Modeling topographic and climatic control of east-west asymmetry in Sierra Nevada glacier length during the Last Glacial Maximum, J. Geophys. Res., 111, F02002, doi:10.1029/2005JF000365, 2006.

Konz, M. and Seibert, J.: On the value of glacier mass balances for hydrological model calibration, J. Hydrol., 385, 238–246, 2010.

Le Meur, E. and Vincent, C.: A two-dimensional shallow ice-flow model of Glacier de Saint-Sorlin, France, J. Glaciol., 49, 527–538, 2003.

Lindström, G., Johansson, B., Persson, M., Gardelin, M., and Bergström, S.: Development and test of the distributed HBV-96 hydrological model, J. Hydrol., 201, 272–288, 1997.

MacGregor, K. R., Anderson, R., Anderson, S., and Waddington, E.: Numerical simulations of glacial-valley longitudinal profile evolution, Geology, 28, 1031–1034, 2000.

Mann, H. B.: Nonparametric tests against trend, Econometrica, J. Econom. Soc., 13, 245–259, 1945.

Marshall, S. J., White, E. C., Demuth, M. N., Bolch, T., Wheate, R., Menounos, B., Beedle, M. J., and Shea, J. M.: Glacier water resources on the eastern slopes of the Canadian Rocky Mountains, Can. Water Resour. J., 36, 109–134, 2011.

Martinec, J.: New methods in snowmelt-runoff studies in representative basins, in: IAHS Symposium on Hydrological Characteristics of River Basins, IAHS Publ. No. 117, 99–107, 1975.

Moore, R., Fleming, S., Menounos, B., Wheate, R., Fountain, A., Stahl, K., Holm, K. and Jakob, M.: Glacier change in western North America: influences on hydrology, geomorphic hazards and water quality, Hydrol. Process., 23, 42–61, 2009.

Nash, J. and Sutcliffe, J.: River flow forecasting through conceptual models part I – A discussion of principles, J. Hydrol., 10, 282–290, 1970.

Nijssen, B., Schnur, R., and Lettenmaier, D. P.: Global retrospective estimation of soil moisture using the variable infiltration capacity land surface model, 1980–93, J. Climate, 14, 1790–1808, 2001.

Plummer, M. A. and Phillips, F. M.: A 2-D numerical model of snow/ice energy balance and ice flow for paleoclimatic interpretation of glacial geomorphic features, Quaternary Sci. Rev., 22, 1389–1406, 2003.

Press, W. H., Teukolsky, S. A., Vetterling, W. T., and Flannery, B. P.: Numerical Recipes, 3rd Edn., The Art of Scientific Computing, Cambridge University Press, 2007.

Racoviteanu, A. E., Williams, M. W., and Barry, R. G.: Optical remote sensing of glacier characteristics: a review with focus on the Himalaya, Sensors, 8, 3355–3383, 2008.

Radić, V. and Hock, R.: Regionally differentiated contribution of mountain glaciers and ice caps to future sea-level rise, Nat. Geosci., 4, 91–94, 2011.

Rees, H. G. and Collins, D. N.: Regional differences in response of flow in glacier-fed Himalayan rivers to climatic warming, Hydrol. Process., 20, 2157–2169, 2006.

Schäfer, M. and Le Meur, E.: Improvement of a 2-D SIA ice-flow model: application to Glacier de Saint-Sorlin, France, J. Glaciol., 53, 713–722, 2007.

Schaefli, B. and Huss, M.: Integrating point glacier mass balance observations into hydrologic model identification, Hydrol. Earth Syst. Sci., 15, 1227–1241, doi:10.5194/hess-15-1227-2011, 2011.

Schindler, D. and Donahue, W. F.: An impending water crisis in Canada's western prairie provinces, P. Natl. Acad. Sci. USA, 103, 7210–7216, 2006.

Sen, P. K.: Estimates of the regression coefficient based on Kendall's tau, J. Am. Stat. Assoc., 63, 1379–1389, 1968.

Singh, P. and Bengtsson, L.: Hydrological sensitivity of a large Himalayan basin to climate change, Hydrol. Process., 18, 2363–2385, 2004.

Stahl, K. and Moore, R.: Influence of watershed glacier coverage on summer streamflow in British Columbia, Canada, Water Resour. Res., 42, 1–5, 2006.

Stahl, K., Moore, R., Shea, J., Hutchinson, D., and Cannon, A.: Coupled modelling of glacier and streamflow response to future climate scenarios, Water Resour. Res., 44, W02422, doi:10.1029/2007WR005956, 2008.

Storck, P.: Trees, Snow and Flooding: an Investigation of Forest Canopy Effects on Snow Accumulation and Melt at the Plot and Watershed Scales in the Pacific Northwest, Ph.D. thesis, University of Washington, 2000.

Storck, P., Bowling, L., Wetherbee, P., and Lettenmaier, D.: Application of a GIS – based distributed hydrology model for prediction of forest harvest effects on peak stream flow in the Pacific Northwest, Hydrol. Process., 12, 889–904, 1998.

Thyer, M., Beckers, J., Spittlehouse, D., Alila, Y., and Winkler, R.: Diagnosing a distributed hydrologic model for two high-elevation forested catchments based on detailed stand-and basin-scale data, Water Resour. Res., 40, W01103, doi:10.1029/2003WR002414, 2004.

Weertman, J.: On the sliding of glaciers, J. Glaciol., 3, 33–38, 1957.

Wendell, V. T.: The effect of glaciers on streamflow variations, Water Resour. Res., 21, 579–586, 1985.

Whitaker, A., Alila, Y., Beckers, J., and Toews, D.: Application of the distributed hydrology soil vegetation model to Redfish Creek, British Columbia: model evaluation using internal catchment data, Hydrol. Process., 17, 199–224, 2003.

Wigmosta, M. S., Vail, L. W., and Lettenmaier, D. P.: A distributed hydrology-vegetation model for complex terrain, Water Resour. Res., 30, 1665–1680, 1994.

WGMS.: Glacier Mass Balance Bulletin No. 10 (2006–2007), edited by: Haeberli, W., Gärtner-Roer, I., Hoelzle, M., Paul, F., and Zemp, M., ICSU(WDS)/IUGG(IACS)/UNEP/UNESCO/WMO, World Glacier Monitoring Service, Zurich, 2009.

Modeling the effect of glacier recession on streamflow response

B. S. Naz et al.

Title Page

Abstract | Introduction

Conclusions | References

Tables | Figures

◀ | ▶

◀ | ▶

Back | Close

Full Screen / Esc

Printer-friendly Version

Interactive Discussion

Table 1. Calibrated DHSVM parameters.

Parameter	Initial value	Analyzed range	Calibrated
Lateral conductivity	0.01	1.0e-6–0.01	1.5e-3
Exp. decrease	2.0	1–3	2.5
Snow roughness	0.005	1.0e-5–0.01	0.005
Precipitation lapse rate ($m\,m^{-1}$)	0.0012	0.001–0.0001	0.0002
Temperature lapse rate	−0.0065	−0.0075–0.0	−0.0070

Table 2. Monthly and daily Nash values for simulated streamflow. Values in parentheses indicate model performance without the glacier model.

Time period	N.S.E monthly	N.S.E. daily
Calibration (odd years)	0.83 (0.70)	0.70 (0.57)
Validation (even years)	0.83 (0.73)	0.73 (0.65)
Entire period (1981–2008)	0.82 (0.70)	0.72 (0.61)

Table 3. Trend statistics and trend slopes computed with the Sen's slope estimator for the time period 1980–2007. Slopes of statistically significant trends are in bold.

	Positive degree days (pdd yr^{-1})	Mean annual temperature (°C yr^{-1})	Annual precipitation (mm yr^{-1})	Simulated annual runoff		Simulated runoff (May–Oct)	
				Total (mm yr^{-1})	Glacier contribution (% yr^{-1})	Total (mm yr^{-1})	Glacier contribution (% yr^{-1})
Mann–Kendall (Sen Slope)	**0.38**	**0.08**	−0.04	−0.14	0.13	−0.10	0.177
P value	0.0034	0.002	0.49	0.49	0.92	0.92	0.540

Title Page

Abstract | Introduction

Conclusions | References

Tables | Figures

|◄ | ►|

◄ | ►

Back | Close

Full Screen / Esc

Printer-friendly Version

Interactive Discussion

Table A1. Dates of acquisition of Landsat 5 scenes used in this study.

No	Landsat 5 TM
1	28 Aug 1986
2	27 Sep 1991
3	2 Aug 1994
4	7 Sep 1998
5	15 Sep 2001
6	13 Aug 2004
7	16 Sep 2007
8	12 Sep 2009
9	26 Aug 2011

Title Page

Abstract   Introduction

Conclusions   References

Tables   Figures

⏮   ⏭

◀   ▶

Back   Close

Full Screen / Esc

Printer-friendly Version

Interactive Discussion
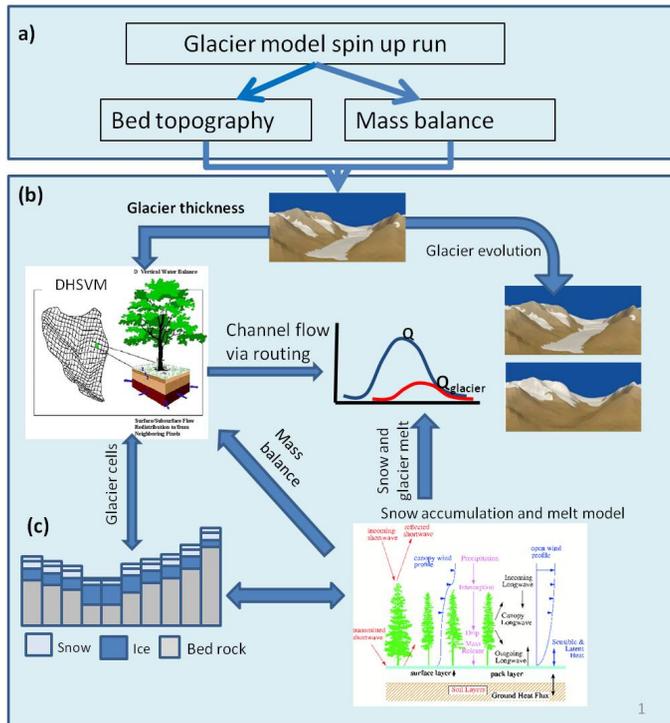
Fig. 1. Schematic of integrated DHSVM and glacier flow model: **(a)** glacier model initialization to estimate ice thickness; **(b)** DHSVM full energy and mass balance snow model; and **(c)** schematic of a glacier illustrating the introduction of a third layer to represent glacier in a two-layer snow model.
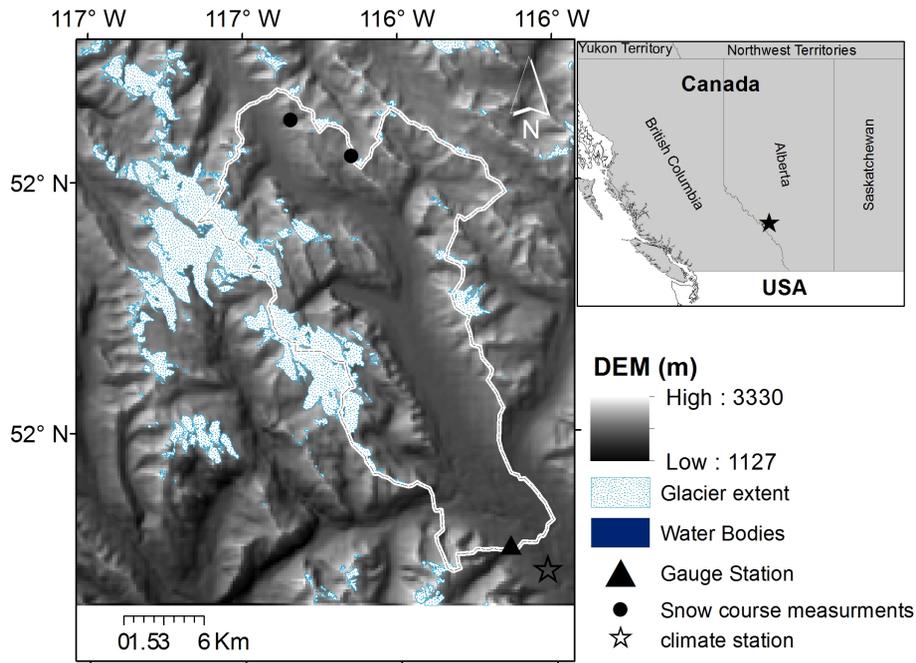
Fig. 2. Location of the Upper Bow River basin, stream gauging station above Lake Louise, snow course and Lake Louise climate station locations. Glacier cover is based on the Landsat image acquired on 26 August 1986.

Full Screen / Esc

Printer-friendly Version

Interactive Discussion
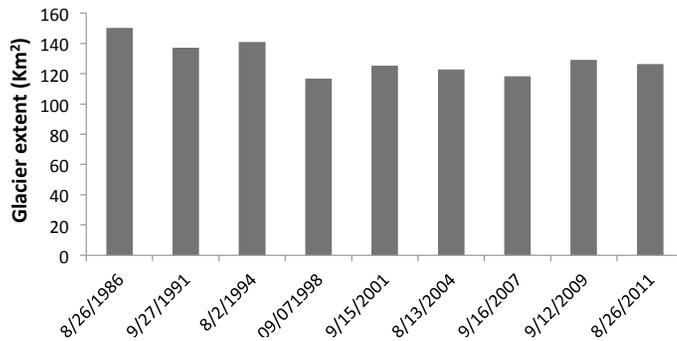
Fig. 3. Change in Landsat-derived glacier extent in the Bow River basin, 1986–2011.
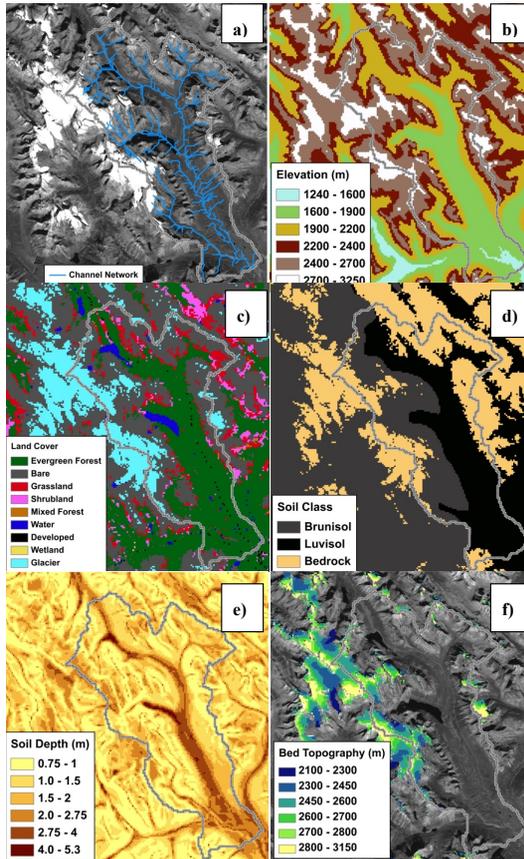
Fig. 4. Input data sets used in the study: **(a)** DEM-derived stream network; **(b)** 90 m SRTM DEM; **(c)** land cover classes; **(d)** soil classes; **(e)** Spatial distribution of DEM-derived soil depth; **(f)** subglacial topography.
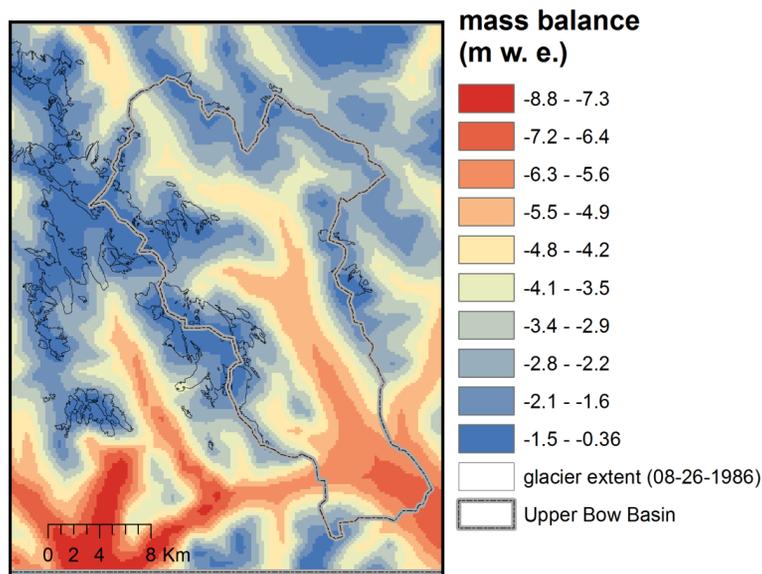
Fig. 5. Spatial distribution of average net mass balance ($\mathrm{m\,yr^{-1}}$) estimated using 1 km down-scaled NARR precipitation and temperature data for the time period 1979–2008 based on temperature index model with $3.9\,\mathrm{mm\,d^{-1}\,{}^{\circ}C^{-1}}$ degree day factor.
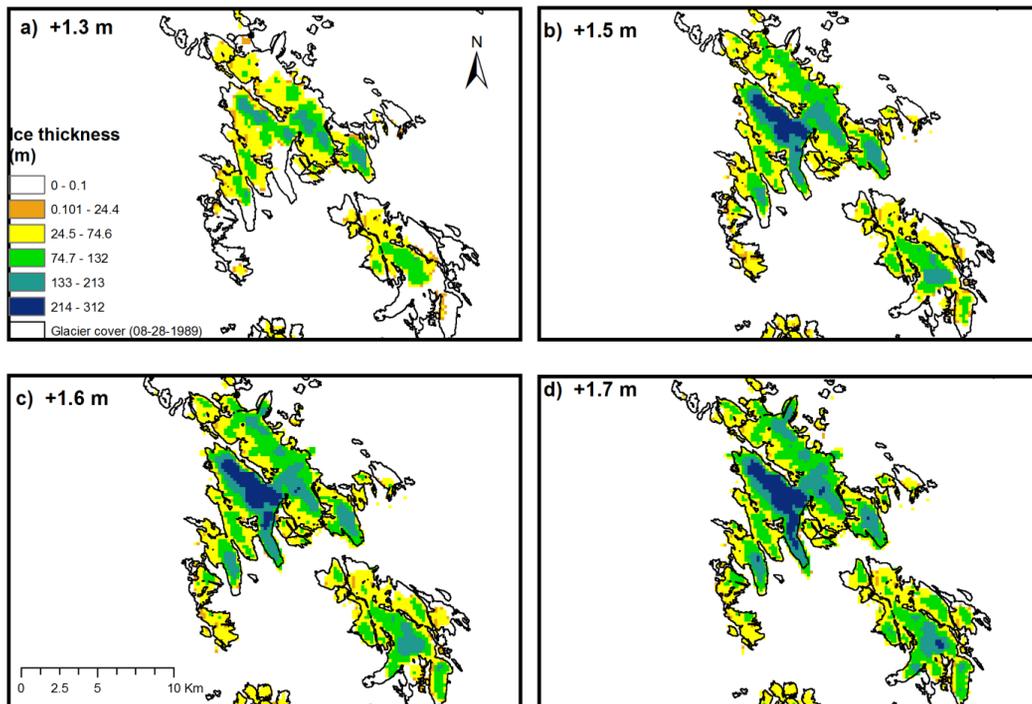
Fig. 6. Steady-state ice thickness distributions corresponding to increases (m w.e. yr^{-1}) applied to averaged 1979–2008 net mass balance shown in Fig. 5. The numbers indicate the increases applied to averaged mass balance only within glacierized areas. Glacier cover extents were delineated from the Landsat image acquired 26 August 1986.
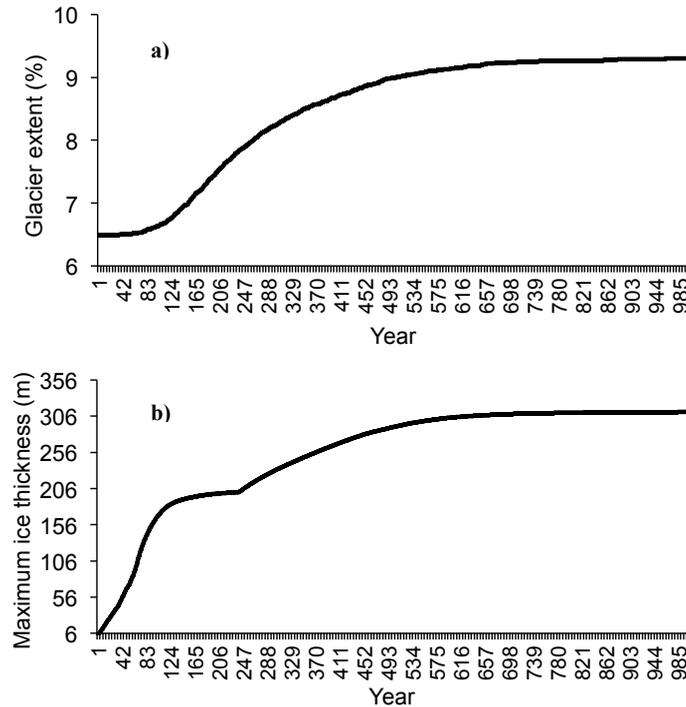
Fig. 7. Development of simulated **(a)** glacier extent (%), and **(b)** maximum ice thickness (m) until the glacier reaches the steady state during spin up time period of glacier dynamic model using NARR based 1979–2008 average mass balance field and subglacial topography.
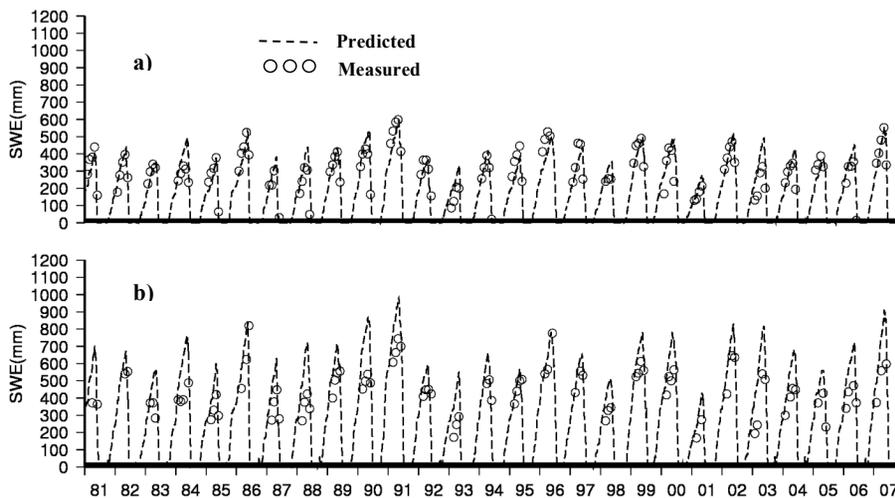
Fig. 8. Measured and modeled predicted SWE for two locations in the upper Bow River basin; **(a)** Bow Summit at elevation (2080 m a.s.l.); **(b)** Katherine Lake (2380 m a.s.l.).

Full Screen / Esc
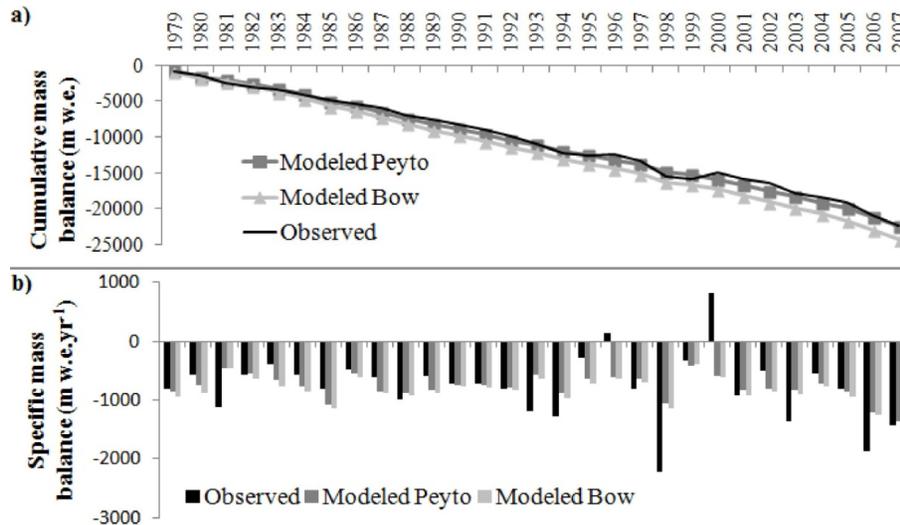
Fig. 9. Model performance evaluation of predicted glacier mass balance with observed measurements on Peyto glacier for period of 1979–2007 through comparison of **(a)** cumulative mass balance and **(b)** annual specific mass balance. Modeled cumulative and annual specific mass balance for Bow glacier are also shown for comparison.
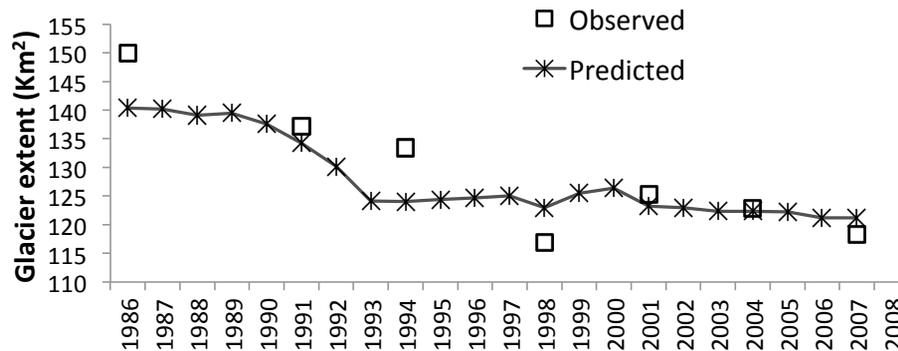
Fig. 10. Comparison of monthly model-predicted ice cover extent with Landsat-derived ice cover for years when the cloud-free images were available at the end of melting season for the study domain. The dates of acquisition of Landsat images are shown in Fig. 3.
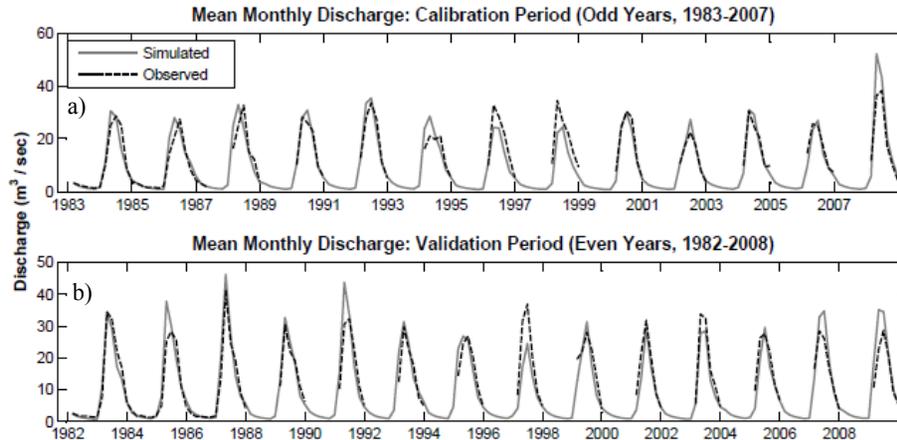
Fig. 11. Comparison of monthly simulated streamflow with observed at Lake Louise gauge station for **(a)** calibration, and **(b)** validation years. The daily observed streamflow data were only available from May–October from 1987 on.
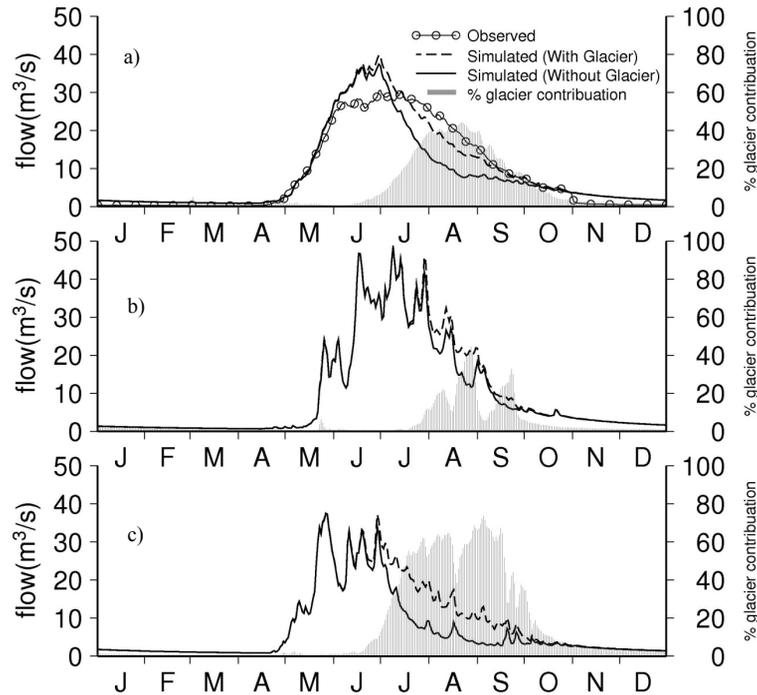
Fig. 12. Comparison of simulated mean annual daily discharge with and without glacier option along with glacier melt contribution in the upper Bow River basin for **(a)** 1980–2007, **(b)** cold year (1999) and **(c)** warm year (1998). The daily observed streamflow data were only recorded from May–October since 1987.